Modeling the Manually Controlled Bicycle

Ronald Hess, *Senior Member IEEE,* Jason K. Moore, and Mont Hubbard

Abstract- **A control-theoretic model of the bicycle rider is developed. The model has its origins in pilot modeling efforts previously reported in the literature. A handling qualities metric that was employed in pilot/vehicle analysis is adopted for use in estimating the task-independent handling qualities of bicycles. The resulting model is parameterized by five gains, two fixed second-order filters, and a preview time. An analysis and computer simulation of the rider/bicycle system is undertaken using six linear models of existing bicycles at three different velocities. The rider's task consisted of a 2 m lane change maneuver and return. Lane tracking performance was comparable for all bicycles at each velocity. Distinct variations in estimated handling qualities levels were evident in the analysis that indicated bicycle velocities rather than differences in the bicycles themselves, dominated the handling qualities predictions. A brief discussion of a rider control model for hands-free riding and a possible approach for model identification concludes the study.**

Index Terms-manual control, human operator modeling, bicycle dynamics

I. Introduction

The bicycle with a human rider comprises a human-vehicle system whose dynamic behavior is poorly understood. The reasons for this are varied, but include complex kinematic vehicle constraints, tire-roadway interactions, and difficulty in realistically modeling relevant human behavior. One result of these complications is that the voluminous research modeling the bicycle over the last century has resulted in no useful design guidelines for the construction of bicycles with desired handling qualities. Even the simplest models of a bicycle with a rigidly attached rider have yet to be adequately understood. Deeper questions regarding the fundamental control methods and objectives of a human rider also remain unanswered and are the key to understanding handling.

Jason Moore is a PhD student in the Department of Mechanical and Aerospace Engineering, University of California, Davis, USA 95616 (email: jkmoor@ucdavis.edu).

Ronald Hess and Mont Hubbard are with the Department of Mechanical and Aerospace Engineering, University of California, Davis, USA 95616 (email: rahess@ucdavis.edu, mhubbard@ucdavis.edu)

In controlling a bicycle, the rider utilizes most of the sensory feedback information that is necessary for vehicular control in general, i.e., visual, proprioceptive, and vestibular. The utility of visual feedback is obvious. Less apparent is the importance of proprioceptive feedback, e.g., sensory information about limb position, for stable and effective bicycle control. What differentiates the control task of the bicycle rider from that of the airplane pilot or the automobile driver [1] is the vital nature of all the feedback information just outlined in controlling the vehicle.

The study of the human bicycle rider has the potential to significantly increase the knowledge of the nature of human interaction with dynamic systems in general, and can do so in an experimental setting that is reasonably tractable and economical. In turn, the research can open up the realm of bicycle design to more rigorous and well-defined control engineering principles.

Bicycle stability has been studied for more than a century [2], but only recently have researchers been able to agree upon and document the stability, dynamic response, and characteristics of the simplest bicycle models, constrained to constant velocity circular motion [3,4]. Several researchers have also successfully developed control algorithms, from Linear Quadratic Regulators (LQR) to fuzzy logic systems, capable of stabilizing a bicycle (both theoretically and in practice) using various inputs such as steering torque [5], rider lean [6], and gyroscopic stabilization [7]. Much less is understood about the added complexity that including a rider brings to the problem and, in particular, the identification of control strategies that a human might employ. Only a few studies have touched upon these issues [8-11].

Designers of manually controlled vehicles have consistently sought correlations between the configuration of the vehicle, task performance and ease of control, otherwise known as "handling qualities." Aircraft flight control is one area that has garnered a significant amount of attention regarding the capabilities of the human controller, with U.S. research in the area dating from the mid-1950's [12]. In aircraft applications, handling qualities refer to those qualities or characteristics that determine the ease and precision with which a pilot may complete a given task [13]. Substitute "bicycle" for "aircraft," and "rider" for "pilot" and a workable definition of bicycle handling qualities is evident. Obviously, research into the manual control and handling characteristics of

bicycles has not received the attention and corresponding research support that have been focused upon aircraft. There are, however, two reasons why bicycle manual control and handling qualities are important. First, as has been alluded to in the preceding, the bicycle offers a relatively safe and inexpensive research vehicle whose stable and safe operation requires continuous reliance upon most of the human sensory capabilities. Thus, in and of itself, the bicycle represents a challenging manual control problem, the study of which can shed light on human control capabilities in general. Second, in a more practical sense, an improved understanding of the nature of human interaction with bicycles may lead to improved bicycle designs, i.e., bicycles that handle better at the low speeds favored by the elderly, children and the disabled, high performance handling for racing and handling of unusual bikes, e.g., recumbent, and cargo.

The paper is organized as follows: Section II outlines a simplified pursuit control model of the human pilot that the first author has developed and that has been used in a number of pilot/vehicle analyses. Section III describes an extension of this model to provide a robust control model for a bicycle/rider system. Section IV applies the rider control model in the analysis and computer simulation of a simple lane-change task performed with six models of existing bicycles at three different velocities. Section V discusses a model structure for hands-free riding. Section VI briefly addresses an approach for identification. Section VII provides a discussion of the results and Section VIII draws conclusions of the study.

II. A Simplified Pursuit Control Model of the Human Pilot

A. The Pilot Model

A tractable model of the human pilot has been developed and described in the literature [14] and will form the basis of this study. The model was also applied to the study of multi-axis human control of rotorcraft [15]. What follows in this section borrows heavily on the presentation in the aforementioned references. The modeling procedure allows for the development of human pilot behavioral models in multi-loop flight control tasks in a simplified framework emphasizing frequency-domain synthesis techniques. Beginning with the primary inner-control loops, each control loop is closed using a combination of output-rate feedback and output-error feedback. It was demonstrated that this approach

can accommodate those aircraft vehicle dynamics that can be stabilized by a human pilot. A method for predicting handling qualities levels that would be assigned to a particular vehicle and task is presented. The purpose of introducing this model is not an attempt to skirt the human control modeling issues associated with bicycle control, but to bring coherence to modeling efforts involving the human controller by demonstrating a common signal-processing structure for such models. One can criticize this approach as providing nothing more than an educated guess as regards the rider control model. Obviously, other control paradigms could have been considered, e.g., fuzzy control, e.g. [16]. However, the authors would argue that the simplified control-theoretic paradigm presented here is a result of over 60 years of manual control research, and it has achieved success in many applications

Fig. 1 represents a model of a human pilot in a simple, single-axis tracking task that will serve as a point of departure. In Fig. 1, M and $\dot{M}$ represent the vehicle output and output-rate for the response variable being controlled and C represents the input or desired value of M. G_{nm} represents a highly simplified model of the pilot's neuromuscular dynamics in the limb (arm or leg) that create the control inputs. In [13], this model was given by

$$G_{nm} = \frac{10^2}{s^2 + 2(0.707)10s + 10^2} \tag{1}$$

The gain K_r is chosen with a value that results in a minimum damping ratio of $\zeta_{min} = 0.15$ for any oscillatory mode in the inner, closed-loop transfer function $\dot{M}/R$ in Fig 1. Typically, the oscillatory mode will emanate from the neuromuscular roots. Alternately, K_r can be chosen based upon a Bode plot of the $\dot{M}/R$ transfer function. Here K_r is the value that will yield a 10 dB magnitude difference between the "neuromuscular mode" peak and the mid-frequency magnitude of the transfer function. This was the approach adopted for this study.

The gain K_p is chosen to provide a desired, open-loop crossover frequency for the entire pilot model. The nominal value of this crossover frequency will be 2.0 rad/sec. This value is not arbitrary and represents a reasonable approximation of moderately high-gain pilot control. Further discussion of this choice can be found in [17], where the

sensitivity of closed-loop system bandwidth to changes in open-loop crossover frequency was examined. It was found that for crossover frequencies ω_c less than approximately 2 rad/sec, closed-loop bandwidth became very sensitive to reduction in ω_c. For experimental corroboration, [18] and [19] present crossover frequency values that have been measured in flight test. The reader will note that, for the sake of simplicity, no inceptor force/feel dynamics are included in this model. This will be amended in discussing the bicycle rider control model in Section III.

All realistic piloting tasks require the control of more than one vehicle response variable. For example, the lateral control of a hovering rotorcraft would typically require control of vehicle roll attitude and lateral position relative to a desired hover point. The modeling approach just described can be extended to such tasks, again using the feedback of output rate and output error. The adjustment rules previously defined are merely applied again, with minor changes. Fig. 2 shows a simple multi-loop task.

The notation in Fig. 2 has been deliberately chosen similar to that of Fig. 1. Here the "O" subscript stands for "outer" loop. The C variable in Fig. 2 now serves as the control variable (analogous to δ in Fig.1). For example, Figs. 1 and 2 could represent the lateral hover task just mentioned. Thus, in Fig. 1, $M = \phi$ (vehicle roll attitude) and $C = \phi_C$ (commanded roll attitude). In Fig. 2, $M_O = y$ (vehicle lateral displacement from desired hover point). The closed-loop dynamics evident in the Bode diagram of Fig. 2 assures that the transfer function $\frac{M_O}{C}$ in Fig. 2 will take the form $\frac{M_O}{C}(s) \approx \frac{K}{s}$, thus allowing pure-gain compensation with K_{po} to follow the dictates of the crossover model of the human. Note that the signal U_M, shown in Fig. 1 is now subsumed in the block labeled "vehicle with primary loop closed" in Fig. 2.

B. Estimation of Handling Qualities

Handling qualities of piloted aircraft are quantified through the use of a rating scale referred to as the Cooper-Harper Pilot Rating Scale [13]. The numerical Cooper-Harper Ratings (CHRs) are typically categorized as "Level 1" (satisfactory) with $1 \leq CHR \leq 3.5$,

"Level 2" (unsatisfactory) with $3.5 < \text{CHR} \leq 6.5$, and "Level 3" (unacceptable) with CHR > 6.5. The definition of Level 3 can vary, but here the definition just given will suffice.

The research summarized in [20] hypothesized that a pilot's perception of task difficulty, and therefore, of vehicle handling qualities was solely dependent upon the amount of "power" in the output-rate feedback signal in a model such as that of Fig. 1. The structural model of the pilot discussed in [21] and [22] proposed a similar model-derived measure, i.e., a handling qualities sensitivity function (HQSF). Rather than concentrating on the power in the output-rate feedback signal, the HQSF focused on how this feedback signal was created in the model. A similar metric is proposed in the model presented here. That is, it is proposed that task-independent handling qualities can be reflected in the maximum magnitude of the transfer function between the inner-loop rate feedback variable U_M and the command input C. Thus, a task-independent handling qualities metric (HQM) can be defined as

$$\text{HQM} = \left| \frac{U_M}{C}(j\omega) \right| \cdot \frac{1}{|K_p|} \quad 1/\text{sec} \tag{2}$$

The HQM obviously reflects the power in U_M. The normalization by $|K_p|$ apparent in Eq. 2 is important as it removes the effects of control sensitivity on handling qualities assessment. Fig. 3 shows the HQMs for a series of controlled elements identified in the legend. The task for which objective ratings were obtained was a single-axis, compensatory, laboratory tracking task emulating aircraft roll control. The subjects were controlling dynamics of the form shown in the figure legend using an aircraft control stick. The forcing function was a random-appearing sum of sinusoids driving an artificial horizon. Details can be found in [23]. Also shown are suggested boundaries between handling qualities levels. These bounds have been assigned after reviewing the handling qualities ratings assigned to the controlled element dynamics given in the figure. The horizontal bounds shown were selected as the simplest that could be drawn and still delineate between the HQMs shown. Fig. 3 shows that, as perceived handling qualities improve, the peak magnitude of the HQM decreases. This peak also moves to higher frequencies. At these frequencies the power in the command input C would also be

reduced compared to the power existing at the lower frequencies typical of command inputs in a manually controlled system. Both these characteristics would imply a reduction in the total power in the signal U_M, the output-rate feedback signal. It is important to emphasize that use of the bounds of Fig. 3 requires that $\omega_c = 2$ rad/sec. This procedure also assumes that any performance requirements that have been defined in the task description have been met, and is the reason for describing the estimate as task-independent handling qualities.

C. Command Filtering and Preview

The work of [14] emphasized pilot modeling of vehicles such as rotorcraft in transient maneuvers described in detail in [24]. In these cases, filtering of the command input and a simplified approach to preview was involved. The filter was described by

$$G(s) = \frac{(\omega_{n-filter})^2}{s^2 + 2\omega_{n-filter}s + (\omega_{n-filter})^2} \tag{3}$$

where

$$\omega_{n-filter} = 2.4 \text{ rad/sec} \tag{4}$$

In Eq. 4, the value for $\omega_{n\text{-}filter}$ approximates the crossover frequency of the inner response feedback loop (feedback of M in Fig. 1). Equation 4 ensures that the majority of power in the command signal does not exceed the highest bandwidth control loop in the pilot model.

Preview was accommodated in [14] by the simple expedient of modifying Eq. 3 to read

$$G(s) = \frac{(\omega_{n-filter})^2 \cdot e^{\tau_p s}}{s^2 + 2\omega_{n-filter}s + (\omega_{n-filter})^2} \tag{5}$$

where τ_p represents a preview time. In [25], where a model of an automobile driver was developed and exercised, a similar simplified approach to preview was successfully employed. There, a specific value of τ_p was chosen based upon minimizing phase lags in the closed loop transfer function between command input and response. Obviously, the

approach in Eq. 5 is adopted for expediency and should not be confused with more detailed preview formulations such as those presented in [26].

III. The Bicycle Rider Control Model

A. The Linear Bicycle Model

A description of the development of the linear bicycle model that will be used in this study can be found in [3], where the frame includes the mass and inertia properties of a rigidly attached rider. It cannot be overemphasized at this juncture that the bicycle model to be discussed in a linear representation, including kinematic relations. The definitions that follow refer to the linearized equations that follow:

$$[M]\{\ddot{q}\} + v[C_1]\{\dot{q}\} + (g[K_0] + v^2[K_2])\{q\} = \{f\} \tag{6}$$

where $\{q\} = \begin{Bmatrix} \phi \\ \delta \end{Bmatrix}$ and $\{f\} = \begin{Bmatrix} T_\phi \\ T_\delta \end{Bmatrix}$.

ϕ = bicycle rear frame roll with respect to the vertical, positive clockwise when viewed from behind the frame, rad

δ = handlebar steering input, positive clockwise when viewed from above the frame, rad

T_ϕ = externally applied torque about a line connecting the wheel contact points, positive clockwise when viewed from behind the frame, N-m

T_δ = resultant torque of all rider applied handlebar forces, about the steer axis between the fork and the rider/frame, positive clockwise when viewed from above, N/m

v = bicycle velocity, (assumed constant), m/sec

g = acceleration due to gravity

[M], $[C_1]$, $[K_0]$ and $[K_2]$ = 2 x 2 constant matrices, which are functions of rider and bicycle parameters given in [3].

The Appendix provides numerical values for the elements in these matrices for the six bicycles under consideration, in addition to providing needed kinematic relations for heading and lateral deviation of the front-wheel contact point. In all that follows (up to Section V) $T_\phi = 0$.

B. The Rider Control Model

Fig. 4 shows the rider control model structure for the bicycle frame roll control. It differs from the structure described in Section II by the appearance of an additional, inner-loop featuring feedback of steering input δ through a gain K_δ to a modified form of the G_{nm} from Eq. 1, defined as

$$G_{nm_b} = \frac{30^2}{s^2 + 2(0.707)30s + 30^2} \tag{7}$$

The addition of the δ feedback loop as well as the higher-bandwidth G_{nm_b} were required in order to obtain closed-loop rider/vehicle dynamics with bandwidths sufficient to stabilize the bicycle across the velocity ranges considered. In essence, this loop includes the "force/feel system" dynamics excluded in the model of Fig. 1. Note that only three gains, K_δ, $K_{\dot{\phi}}$, and K_ϕ are required to parameterize the rider control model. The lineage of the model of Fig. 4 with respect to that of Fig. 1 is evident and deliberate. The most likely sensory feedback modalities are also included in Fig. 4. These include feedback from the proprioceptors in the rider's arms, (muscle spindles and joint angle receptors [27]), feedback from the vestibular sensors in the inner-ear, (the semi-circular canals, [28]), and feedback from the visual system. It should be noted that, in keeping with the simplified nature of the representation, models of the sensory systems have not been included. The importance of proprioceptive feedback cannot be overemphasized. The capabilities of haptic feedback in the manual control of dynamic systems is well-known, e.g. [29].

The complete rider/vehicle model, including outer-loop closures (heading ψ and lateral deviation y of the front-wheel contact point from a point on the path) is shown in Fig. 5. The relations for determining heading dynamics and lateral deviation are identical to those used in [3]. In the bicycle models to be considered, ψ is measured from the rear frame roll axis in the ground plane to an arbitrary line on the earth and y is the distance of the front wheel contact point from a desired position on the earth. This "desired position" is one that would be in evidence if one were moving at the nominal bicycle velocity along the command lane-change path.

The added inner-loop closure evident in Fig. 4 as compared to Fig. 1 means that the calculation of the HQM needs to be modified. This was accomplished by simply moving the δ feedback injection point to the differential element where $\dot{\phi}$ is also fed back, with an appropriate gain $(1/K_{\dot{\phi}})$ multiplying δ. The sum of the two signals, $\dot{\phi}+(1/K_{\dot{\phi}})\delta$, then takes the place of $\dot{\phi}$ alone, in the HQM calculation. Finally, the HQM as defined in Eq. 2 was filtered by $20^2/(s+20)^2$. The break frequency of the filter was chosen as a decade beyond the crossover frequency of the ϕ loop and is intended to reduce HQM magnitudes at frequencies where there would be little power in the signal ϕ_c. Care was taken to ensure that this modification did not change the handling qualities level predictions of the controlled elements called out in the legend of Fig. 3.

As an example of selecting the five gain values in Figs. 4 and 5, consider the bicycle model taken from [3] for v = 5 m/sec. For this bicycle (and rigid rider), the matrices involved in Eq. 6 are given by:

$$[M]=\begin{bmatrix}80.8 & 2.32\\ 2.32 & 0.3\end{bmatrix}\quad [K_0]=\begin{bmatrix}-80.9 & -2.6\\ -2.6 & -0.8\end{bmatrix}$$
$$[K_2]=\begin{bmatrix}0 & 76.6\\ 0 & 2.65\end{bmatrix}\qquad [C_1]=\begin{bmatrix}0 & 33.9\\ -0.85 & 1.69\end{bmatrix} \tag{8}$$

Fig. 6 shows the Bode diagrams for the δ and $\dot{\phi}$ closed-loop transfer functions from Fig. 4 and the neuromuscular model from [30]. Note the 10 dB "neuromuscular mode" peaking in the δ and $\dot{\phi}$ loops and the similarity between the model characteristics and that of measured human neuromuscular dynamics from [30]. The model gains were chosen as K_δ = 46.5 N-m/rad and $K_{\dot{\phi}}$ = -0.052 rad/(rad/sec). The 30 rad/sec bandwidth of the system of Eq. 7 may seem high, but this loop and its associated feedback gain K_δ are assumed to be part and parcel of the human's ability to control manipulators. It should not be inferred that the control model developed herein applies only to agile, highly-skilled riders. Fig. 7 shows the Bode diagrams of the of the ϕ, ψ, and y open-loop transfer functions from Fig. 6 with K_ϕ = 12.8 (rad/sec)/rad yielding a 2 rad/sec crossover

frequency, K_ψ = 0.177 rad/rad, yielding a 1 rad/sec crossover frequency, and K_y = 0.097 rad/m (yielding a 0.5 rad/sec crossover frequency. This figure demonstrates that the model exhibits the "classical" neuromuscular mode of the human controller found in nearly all manual control tasks involving the movement of a manipulator, e.g. [27, 30, 31]. Note that the frequency where this mode occurs is approximately 14-15 rad/sec, and considerably smaller than the 30 rad/sec bandwidth of "open-loop" system of Eq. 7. The factor of two separating the crossover frequencies in the ϕ, ψ and y loops is an estimate but is based upon sound, sequential loop-closure design techniques in the frequency domain as applied to manual control [1].

The Bode plots of Fig. 7 are included to emphasize that the rider control model presented herein follows the dictates of the well-established crossover-model of the human operator or controller [32] and does so in each of the primary feedback loops of the model that involve the bicycle response variables ϕ, ψ and y. Finally, Fig. 8 shows the resulting HQM for this bicycle, indicating Level 1 (satisfactory) task-independent handling qualities.

IV Exercising the Model

A. The Bicycle Models and Task

The Appendix provides a description of the six bicycle models that will be used in the study in terms of bicycle physical parameters and the coefficient matrices of Eq. 6. In addition, the rider control model gains for each case (bicycle and velocity) are included. It should be emphasized that the models are based upon six existing bicycles. The rider's task will be to start from a straight-line track and complete a lane change and return consisting of a lateral 2 m translation followed, after 40 m, to a return to the original straight track. Three vehicle velocities will be considered, 2.5 m/sec, 5 m/sec and 7.5 m/sec. The magnitude of the lane change was kept small so as not to invalidate assumptions used in obtaining the linearized bicycle models.

Fig. 9 shows model design results for the six bicycles at v = 5 m/sec that correspond to the ϕ-loop results of Fig. 7 for the bicycle model from [3]. Similar results are obtained for v = 2.5 m/sec and 7.5 m/sec. Fig. 10 shows the HQMs for these bicycles at each of the

velocities considered. The curve labeled “hands-free” relates to a hands-free rider control to be discussed in Section V.

The results of Fig. 10 indicate an overwhelming dependence on bike velocity rather than the particular bike in question in the prediction of handling qualities. Essentially at velocities at or above 5 m/sec, the handling qualities of each bike are within or close to “Level 1”, indicating satisfactory characteristics. A noticeable, difference among bicycles at all velocities can be noted in Fig. 10. At 2.5 m/sec, three of the HQM plots (for bikes 1, 2 and 6) exhibit higher maximum values than those for the remaining three bikes. At 5 and 7.5 m/sec, these differences diminish but are still noticeable for bikes 1 and 2. This would indicate some sensitivity of the HQM to the physical characteristics of the bicycles, themselves.

A plausible reason for the strong dependence of handling qualities upon bike velocity can be offered by Fig. 11 where the real part of the “most unstable” bicycle model eigenvalue (no rider inputs) for each bicycle is shown as a function of velocity. For stable bicycles, the root(s) closest to the imaginary axis was selected. As Fig. 11 clearly shows, stability is a strong function of bike velocity, a phenomenon that has long been known in bicycle research. Taken together, Figs. 10 and 11 suggest a strong correlation between stability and handling. This is not an unusual result. The instabilities at 2.5 m/sec are significant, with times-to-double amplitude of the unstable modes on the order of 0.3 sec. By way of comparison, the study of [23] included controlled element dynamics of the form 1/(s-2), with the unstable mode exhibiting a time-to-double amplitude of 0.35 sec. Although not included in the controlled elements of Fig. 5, these dynamics received Cooper-Harper ratings of 9-10 in the study of [23]. The results of Fig. 10 with the descriptions of the Cooper-Harper scale would indicate that loss of control should be expected with the bicycles at a velocity of 2.5 m/sec. This was not the case in the computer simulations conducted herein, nor is it the case in typical cycling [11]. Probably the most accurate description would be the one associated with a Cooper-Harper rating of 8.0, namely, “considerable pilot (rider) compensation is required for control.”

Note that one bike exhibiting stable roots at 5 m/sec, exhibited slightly unstable roots at 7.5 m/sec (bike 5). This difference had little effect on handling qualities and could be

explained by the fact that the unstable root in question exhibited a time-to-double amplitude of 5.1 sec.

B. Computer Simulation Results

Fig. 12 shows the path tracking results for the six bicycles at the three velocities identified in the previous paragraph. Preview times for all were approximately 2.75 sec and were selected by the simple expedient of adjusting the preview time until simulated tracking performance on the leg of the lane-change maneuver beginning at 50 m was satisfactory. The ordinate of Fig. 12 deserves some comment. To retain readability in displaying each path for each bike at the three velocities, the path tracking time histories were scaled. The ordinate repeatedly showing 2 m is intended to indicate the scaling involved.

Bicycle roll attitudes, steering inputs and steering torques are shown in Figs. 13 – 15. "Counter steering" was evident at the beginning of the maneuvers and is highlighted in Fig. 14 for the 2.5 m/sec velocity. Counter steering refers to the well-known phenomenon in bicycle control in which the handlebars are rotated briefly in a direction counter to the intended direction of travel to initiate a change in direction. The steering torques in Fig. 5 are all relatively small. in magnitude. Note, however, the torque differences between Bikes 5 and 6, occur only because Bike 6 has a reversed fork.

V. A Preliminary Model for Hands-Free Riding

A. A "Zeroth Order" Approximation

The rider control model developed and exercised in the preceding sections would obviously not be suitable for hands-free riding, dependent as it is, upon an inner-most loop closure around the handlebar input. Thus, at least a brief prospectus on how the model might be modified to accommodate the hands-free rider is in order. Fig. 16 shows the proposed structure, which is very similar to that of Fig. 4, except that the aforementioned inner-loop has been removed. Additionally, the input is a moment, T_ϕ, appearing in Eq. 6. T_ϕ is used here under the assumption that it is a moment that mimics the effects of an additional rider lean degree of freedom. It is at this juncture that nature of the hands-free model is evident. Basically, the model formulation will ignore any

changes in the response characteristics of the bicycle-rider combination that accrues with rider lean, save for the moment T_ϕ that mimics the effect of rider lean. This means the bicycle model still uses a rider rigidly affixed to the frame. A more complete model of the hands-free rider would include a proprioceptive feedback loop generating and controlling upper-body lean. This "zeroth order" formulation will depend for its legitimacy upon only small moments being produced (implying minimal rider lean). The remaining loop structure for this model is identical to that shown in Fig. 7.

B. Developing the Hands-Free Model

The hands-free rider control model will be developed in precisely the same manner as the earlier rider models save that analysis shows that lower crossover frequencies are required for stability. The bicycle model of Eq. 8 will again be used. Fig. 17 shows the inner-most loop closure for the new model. Note that, as compared to the $\dot{\phi}$ loop of Fig. 6, the "neuromuscular" mode break frequency occurs at a considerably lower frequency, about 5.5 rad/sec as compared to the 15 rad/sec frequency evident in Fig. 6. As will be seen, this reduction lead to significantly poorer predicted handling qualities than that for the "hands-on" bicycles. Fig. 18 shows the Bode diagram of the ϕ, ψ, and y open-loop transfer functions, corresponding to those shown in Fig. 7. Here the crossover frequencies have been reduced from 2 rad/sec to 1.5 rad/sec for the ϕ loop, 1.0 rad/sec to 0.75 rad/sec for the ψ loop, and 0.5 rad/sec to 0.375 rad/sec for the y loop. The rider control model gain values for the hands-free case, now four in number, are given below:

$$K_{\dot{\phi}} = 55 \text{ N-m/(rad/sec)}, \quad K_\phi = 3.76 \text{ (rad/sec)/rad},$$
$$K_\psi = 0.413 \text{ rad/rad}, \qquad K_y = 0.076 \text{ rad/m} \tag{9}$$

C. Computer Simulation of the Hands-Free Model

Using the same lane-change task as in the previous section, the performance of the rider/bicycle model was examined through a computer simulation. Fig. 19 shows the path tracking performance, roll response, steering and "lean" torque. The maximum magnitudes apparent for lean torque imply small rider lean angles, and would support the approximation that was the underpinning of the simplified hands-free model. The

preview time was increased from the 2.75 sec of the previous models to 3.5 sec for the hands-free case. Although no "counter lean torque" is evident in Fig. 38, an examination of the steering angle resulting from the lean torque indicated counter steering input with hands free. This is shown in Fig. 19. Finally, returning to the HQM results of Fig. 10, the curve identified as "hands-free" is the HQM for the hand-free case, clearly indicates Level 2 handling qualities.

VI. An Approach for Identification

The rider control model structure based upon successive loop structures with single gain elements in each loop (save the inner-most) invites conjecture about possible approaches for rider control model identification from experimental data. The bandwidth of each of the loops in Figs. 4 and 5 determines the relationship between the output of each loop, and the first derivative of that output. The gain element in each of these loops, in turn, determines the bandwidth. This suggests that the shape of phase-plane portraits of the output and its first derivative for each loop may offer a means of approximating the gain value, providing the appropriate output and its first derivative can be measured. Essentially one varies the gain in the loop in question until the phase plane from experiment approximates that obtained from a simulation of the rider/bicycle. Concentrating upon the first three loops of Fig. 4, this means measurement of $(\delta, \dot{\delta})$, $(\dot{\phi}, \ddot{\phi})$, and $(\phi, \dot{\phi})$. Again utilizing the bicycle model of Eq. 8, Fig. 20 shows the variation in the phase plane portraits of each loop that accrue with 20% changes in the indicated gain values. This was done with model-generated data from the lane change maneuver. The figure indicates that as one moves from the inner to outer loop in Fig. 4 (a – c), the phase portraits become increasingly sensitive to changes in the gain values for the loop in question. The fact that the inner-most loop is fairly insensitive to gain changes is encouraging from the standpoint of phase-plane "identification" as this is the loop most likely to be corrupted by human rider "remnant," i.e., injected noise [1]. This lack of sensitivity also implies that the particular parameters used in the neuromuscular model of that loop may be of secondary importance. The technique just espoused for model gain approximation has been utilized in human pilot modeling studies, albeit not for identification purposes, e.g., [33]. The gains used in the remaining two loops in the model

simulation (ψ and y) would be the nominal values used in the analysis. This would undoubtedly involve some error. The effect of such an error is demonstrated in Fig. 20(d), where the simulations used for Fig. 20(c) are repeated, but with the K_ψ and K_y gains each reduced by 20%. A comparison of Figs. 20(c) and 20(d) indicate that the basic shapes are retained, but the portraits differ in area.

The proposed identification technique would begin with the bicycle and rider completing a task such as the lane change described here. Measurements of the output and rate pairs identified in the preceding paragraph would be undertaken. With a model of the bicycle and rider as developed here, the analyst would begin from the inner-most loop and select the K_δ that allows the model-derived phase portrait to match that found from experiment as closely as possible This process would continue in the remaining two loops selecting $K_{\dot{\phi}}$ and K_ϕ, respectively. It is obvious that this is not a true "identification" technique as much as a "model-matching" exercise using the rider control model developed herein. Nonetheless, it suggests an avenue for bringing experimental results to bear on rider control model gains.

VII. Discussion

The model described herein should be interpreted as a relatively simple control-theoretic structure that can explain the control behavior of the bicycle rider. The model maintains a lineage with human operator models that have adequately explained the control behavior of humans in other scenarios and tasks, e.g., multi-loop, multi-axis piloted control of aircraft. It should be noted that the model does not attempt to capture higher levels of rider skill development that would fall into the category of "precognitive" behavior, e.g., [34]. Given the simplified nature of the model it is encouraging to note that a single rider control model architecture can stabilize and control a set of bicycle models whose dynamics range from those exhibiting stable eigenvalues (e.g., bicycle 6 at 7.5 m/sec) to ones that exhibit unstable poles and modal responses with times-to-double-amplitude on the order of 0.3 sec (e.g., bicycle 1 at 2.5 m/sec). It is suggested that the rider control model can be used as an analytical tool for the preliminary assessment of bicycle

performance and handling, and to provide an architecture to guide rider/vehicle identification studies.

An examination of the rider control model's ability to discriminate handling qualities differences among different bicycle designs (bicycle physical parameters) was beyond the scope of this initial study. As mentioned in Section IV. A, as compared to the remaining bikes, predicted handling qualities differences were noted in bikes 1, 2 and 6 at 2.5 m/sec and bikes 1, 2 at 5 at 7.5 m/sec. The issue of using the handling qualities predictions for design remains a subject for future research.

VIII. Conclusions

(1) A simplified, control-theoretic model of the bicycle rider has been developed that derives from similar models employed in the study of piloted aircraft flight control.

(2) The bicycle rider control model contains only five gain values, two fixed second-order filter elements and a preview time.

(3) A handing qualities metric derived for the analysis of aircraft flight control can be modified to provide estimates of task-independent handling qualities levels.

(4) The handling qualities metric indicated a strong correlation between the stability of the bicycle and the predicted handling qualities. This correlation far exceeded differences attributable to differences in the six bicycles employed in the study.

(5) Benchmark measures of rider/bicycle performance could be estimated in computer simulations of six bicycle models at three velocities in a lane-change task.

(6) A "zeroth order" approximation for the hands-free model was developed from the model that required rider steering inputs.

(7) A technique for estimating rider control model gains was proposed, based upon the sequential loop structure and simple gain compensation exhibited by the model.

(8) The model can serve as a preliminary assessment tool for analyzing rider/vehicle performance and to guide rider/vehicle identification studies.

(9) Examining the ability of the model to successfully discriminate handling qualities variations attributable to different bicycle designs remains a subject for future research.

Acknowledgment

The research reported herein was sponsored by grant NSF CMMI-0928339 from the National Science Foundation. The authors are grateful to Dale L. Peterson of the UC Davis Sports Biomechanics Laboratory for providing assistance in the preparation of this manuscript.

References

[1] Hess, R. A., "Feedback Control Models," in *Handbook of Human Factors,* Wiley, Editor: G. Salvendy, 1987, pp. 1212 – 1242 (invited chapter).

[2] Whipple, F. J. W., "The Stability of the Motion of a Bicycle," *Quarterly Journal of Pure and Applied Mathematics,* Vol. 30, pp. 312-348, 1899.

[3] Meijaard, J. P., Papadopoulos, J. M., Ruina, A., and Schwab, A. L., "Linearized Dynamics Equations for the Balance and Steer of a Bicycle: A Benchmark and Review," *Proceedings of the Royal Society A: Mathematical, Physical and Engineering Sciences,* Vol. 463, No. 2084, pp. 1955-1982, 2007.

[4] Basu-Mandal, P., Chatterjee, A., and Papadopoulos, J. M., "Hands-Free Circular Motions of a Benchmark Bicycle," *Proceedings of the Royal Society A: Mathematical, Physical and Engineering Sciences,* Vol. 463, No. 2084, pp. 1983-2003, 2007.

[5] Fajans, J., "Steering in Bicycles and Motorcycles," *American Journal of Physics,* Vol. 68, No. 7, pp. 654-659, (2000).

[6] Van Zytveld, P. J., "A Method for the Automatic Stabilization of an Unmanned Bicycle," Engineer's Thesis, Dept. of Aeronautics and Astronautics, Stanford University, Stanford, CA, 1975.

[7] Gallaspy, J. "Gyroscopic Stabilization of an Unmanned Bicycle." Ph.D. Thesis, Auburn University, 2000.

[8] Roland, R. D., and Lynch, J. P., "Bicycle Dynamics Tire Characteristics and Rider Modeling," Technical Report YA-3063-K-2, Cornell Aeronautical Laboratory, Inc. Buffalo, NY, 1972.

[9] van Lunteren, A., and Stassen, H., "On the Variance of the Bicycle Rider's Behavior," *Proceedings of the 6th Annual Conference on Manual Control,* Wright-Patterson AFB, OH, 7-9 April, 1970, pp. 701-722.

[10] Doyle, A. J. R., "The Essential Contribution to Bicycle Riding," *Training, Human Decision Making, and Control,* Elsevier, North Holland, 1988, pp. 351-370.

[11] Moore, J. K., Kooijman, J. D. G., and Schwab, A. L., and Hubbard, M. "Rider Motion Identification During Normal Bicycling By Means of Principal Component Analysis," *Multibody Systems Dynamics*, Vol. 25, No. 2, pp 225-244, 2011.

[12] Anon., "The Human Pilot," US Navy Bureau of Aeronautics, BU AER Report AE-61-4 III, Aug. 1954.

[13] Cooper, G. E., and Harper, R. P., Jr., "The Use of Pilot Rating Scales in the Evaluation of Aircraft Handling Qualities," NASA TN D-5153, April 1969.

[14] Hess, R. A., "Simplified approach for Modelling Pilot Pursuit Control Behaviour in Multi-Loop Flight Control Tasks," *Proceedings of the Institution of Mechanical Engineers, Part G, Journal of Aerospace Engineering,* Vol. 220, No. G2, April 2006, pp. 85-102.

[15] Hess, R. A., "Analytical Assessment of Performance, Handling Qualities, and Added Dynamics in Rotorcraft Flight Control," *IEEE Transactions on Systems, Man, and Cybernetics, Part A: Systems and Humans,* Vol. 39, No. 1, Jan. 2009, pp. 262-271.

[16] Liu, Y.-J., Want, W., Tong, S.-C., and Liu, Y.-S., "Robust Adaptive Tracking Control for Nonlinear Systems Based on Bounds of Fuzzy Approximation Parameters," *IEEE Transactions on Systems, Man, and Cybernetics, Part A: Systems and Humans,* Vol. 40, No. 1, Jan. 2010, pp. 170-184.

[17] Hess, R. A.**,** "Analysis of Aircraft Attitude Control Systems Prone to Pilot-Induced Oscillations," J. *Guidance, Control, and Dynamics,* Vol. 7, No. 1, pp. 106-112, 1984.

[18] Hess, R. A**.,** "Identification of Pilot-Vehicle Dynamics From Simulation and Flight Test, *Control and Dynamic Systems,* Vol. 33*, Advances in Aerospace Systems Dynamics and Control Systems,* Edited by C. T. Leondes, Academic Press, London, 1990, pp. 151-175.

[19] Mitchell, D.G. Aponso, B. L, and Klyde, D. H.**,** "Effects of Cockpit Lateral Stick Characteristics on Handling Qualities and Pilot Dynamics," NASA CR 4443, June 1992.

[20] Smith, R. H., "A Theory for Handling Qualities With Applications to MIL-F-8785B," AFFDL-TR-75-119, Air Force Flight Dynamics Lab., WPAFB, OH, Oct. 1976.

[21] Hess, R. A., Zeyada, Y., and Heffley, R. K., **"**Modeling and Simulation for Helicopter Task Analysis," *Journal of the American Helicopter Society*, Vol. 47, No. 4. pp. 243-252, 2002

[22] Zeyada, Y., and Hess, R. A., "Computer-Aided Assessment of Flight Simulator Fidelity," *Journal of Aircraft,* Vol. 40, No. 1, pp. 173-180, 2003.

[23] McDonnell, J. D.**,** "Pilot Rating Techniques for the Estimation and Evaluation of Handling Qualities," AFFDL-TR-68-76, Air Force Flight Dynamics Lab., WPAFB, OH, Dec. 1968.

[24] Anon., ADS-33E-PRF, Aeronautical Design Standards, Performance Specification, Handling Qualities Design Requirements for Military Rotorcraft, U. S. Army Aviation and Missile command, Redstone Arsenal, AL, March 2000.

[25] Modjtahedzadeh, A., and Hess, R. A., "A Model of Driver Steering Control Behavior for Use in Assessing Vehicle Handling Qualities," *Transactions of the ASME, Journal of Dynamic Systems, Measurement, and Control,* Vol. 115, No. 3, Sept. pp. 456-464, 1993.

[26] Sharp, R. S., "On the Stability and Control of the Bicycle," *Transactions of the ASME, Applied Mechanics Reviews,* Vol. 61, pp. 060803-1 – 060803-24.

[27] Magdaleno, R. E., and McRuer, D. T., "Experimental Validation and Analytical Elaboration for Models of the Pilot's Neuromuscular Subsystem in Tracking Tasks," NASA CR-1757, April, 1971.

007.

[28] Young, L. R., "Spatial Orientation," in *Principles and Practice of Aviation Psychology,* Eds: P. S. Tsang nad M. A. Vidulich, CRC Press, Boca Raton, FL, Chap. 3, 2003.

[29] Mulder, M., Pauwelussen. J. J. A., van Paassen, M. M., Mulder, M., and Abbink, D. A., "Active Deceleration Support in Car Following," *IEEE Transactions on Systems, Man, and Cybernetics, Part A: Systems and Humans,* Vol. 40, No. 6, Nov. 2010, pp. 1271-1284.

[30] McRuer, D. T., Magdaleno, R. E., and Moore, G. P., "A Neuromuscular Actuation System Model," *IEEE Transactions on Man-Machine Systems*, Vol. MMS-9, No. 3, 1968, pp. 61-71.

[31] Hess, R. A., "Analyzing Manipulator and Feel System Effects in Aircraft Flight Control," *IEEE Transactions on Systems, Man, and Cybernetics*, Vol. SMC-20, No. 4, 1990, pp. 923-931.

[32] McRuer, D. T, and Krendel, E., "Mathematical Models of Human Pilot Behavior," AGARDograph No. 188, 1974.

[33] Hess, R. A., and Gao, C., "Generalized Algorithm for Inverse Simulation Applied to Rotorcraft Maneuvering Flight," *Journal of the American Helicopter Society,* Vol. 38, No. 4, 1993, pp. 3-15.

[34] Hess, R.A., "Pursuit Tracking and Higher-Levels of Skill Development in the Human Pilot," *IEEE Transactions on Systems, Man, and Cybernetics,* Vol. SMC-11, No. 4, pp. 262-273, April, 1981.

Appendix

Fig. A1, below, from [A1] defines the basic geometry of the bicycle models to be described. The notation and definitions follow those of [A1]. Table A1 lists the parameter values for each of the bikes. Table A2 lists the rider model parameters.

Parameter Definitions

c = trail, m

r_R = rear wheel radius, m

r_F = front wheel radius, m

v = bike velocity, m/sec

w = wheel base, m

IR_{xx} = rear wheel moment of inertia, kg-m^2

IR_{yy} = rear wheel moment of inertia, kg-m^2

IB_{xx} = rider and rear frame assembly moment of inertia, kg-m^2

IB_{yy} = rider and rear frame assembly moment of inertia, kg-m^2

IB_{zz} = rider and rear frame assembly moment of inertia, kg-m^2

IB_{xz} = rider and rear frame assembly product of inertia, kg-m^2

IF_{xx} = front wheel moment of inertia, kg-m^2

IF_{yy} = front wheel moment of inertia, kg-m^2

IH_{xx} = front handle bar and fork assembly moment of inertia, kg-m^2

IH_{yy} = front handle bar and fork assembly moment of inertia, kg-m^2

IH_{zz} = front handle bar and fork assembly moment of inertia, kg-m^2

IH_{xz} = front handle bar and fork assembly product of inertia, kg-m^2

m_B = rear body and frame mass, kg

m_F = front wheel mass, kg

m_H = handlebar and fork assembly mass, kg

m_R = rear wheel mass, kg

x_B = rider and rear frame center of mass position, m

z_B = rider and rear frame center of mass position, m

x_H = front handle bar and fork center of mass position, m

z_H = front handle bar and fork center of mass position, m

λ = steer axis tilt, rad

Bike 1

Bike 2

Bike 3

Bike 4

Bike 5

Bike 6

Bike 1: Bike 2 which has been instrumented; notably a ~5 kg mass on the rear rack.

Bike 2: Batavus Browser: A Dutch-style city bicycle.

Bike 3: Bianchi Pista: A steel frame track-racing bike.

Bike 4: Gary Fisher: A modern performance hardtail aluminum mountain bike.

Bike 5: Yellow Bike: A stripped aluminum road-racing bike.

Bike 6: Bike 5 in which the fork has been reversed.

Bicycle Equations of Motion

$$[M]\{\ddot{q}\} + v[C_1]\{\dot{q}\} + (g[K_0] + v^2[K_2])\{q\} = \{f\}$$

$$\{q\} = \begin{Bmatrix} \phi \\ \delta \end{Bmatrix} \text{ and } \{f\} = \begin{Bmatrix} T_\phi \\ T_\delta \end{Bmatrix}$$

$$\dot{\psi} = \frac{v\delta + c\dot{\delta}}{w}\cos\lambda \qquad y = y_r + w\psi - c\delta\cos\lambda \qquad \dot{y}_r = v\psi$$

where y_r is the rear-wheel contact point. Equations are taken from [A1].

Bicycle 1

$$[M] = \begin{bmatrix} 106 & 1.55 \\ 1.55 & 0.25 \end{bmatrix} \quad [C_1] = \begin{bmatrix} 0 & 29.9 \\ -0.45 & 1.08 \end{bmatrix} \quad [K_0] = \begin{bmatrix} -93.2 & -1.76 \\ -1.76 & -0.68 \end{bmatrix}$$

$$[K_2] = \begin{bmatrix} 0. & 77.3 \\ 0. & 1.58 \end{bmatrix}$$

Bicycle 2

$$[M] = \begin{bmatrix} 103 & 1.54 \\ 1.54 & 0.25 \end{bmatrix} \quad [C_1] = \begin{bmatrix} 0 & 26.4 \\ -0.45 & 1.04 \end{bmatrix} \quad [K_0] = \begin{bmatrix} -89.3 & -1.74 \\ -1.74 & -0.68 \end{bmatrix}$$

$$[K_2] = \begin{bmatrix} 0. & 74.1 \\ 0. & 1.57 \end{bmatrix}$$

Bicycle 3

$$[M] = \begin{bmatrix} 99.6 & 1.61 \\ 1.61 & 0.19 \end{bmatrix} \quad [C_1] = \begin{bmatrix} 0 & 29.0 \\ -0.34 & 1.12 \end{bmatrix} \quad [K_0] = \begin{bmatrix} -84.6 & -1.77 \\ -1.77 & -0.48 \end{bmatrix}$$

$$[K_2] = \begin{bmatrix} 0. & 82.9 \\ 0. & 1.80 \end{bmatrix}$$

Bicycle 4

$$[M]=\begin{bmatrix}99.9 & 1.73\\ 1.73 & 0.187\end{bmatrix}\quad [C_1]=\begin{bmatrix}0 & 27.4\\ -0.34 & 1.14\end{bmatrix}\quad [K_0]=\begin{bmatrix}-85.1 & -1.91\\ -1.91 & -0.62\end{bmatrix}$$

$$[K_2]=\begin{bmatrix}0. & 75.8\\ 0. & 1.78\end{bmatrix}$$

Bicycle 5

$$[M]=\begin{bmatrix}100 & 1.22\\ 1.22 & 0.18\end{bmatrix}\quad [C_1]=\begin{bmatrix}0 & 25.6\\ -0.45 & 0.87\end{bmatrix}\quad [K_0]=\begin{bmatrix}-85.3 & -1.35\\ -1.35 & -0.40\end{bmatrix}$$

$$[K_2]=\begin{bmatrix}0. & 75.6\\ 0. & 1.30\end{bmatrix}$$

Bicycle 6

$$[M]=\begin{bmatrix}100 & 4.35\\ 4.35 & 0.56\end{bmatrix}\quad [C_1]=\begin{bmatrix}0 & 38.9\\ -0.55 & 3.08\end{bmatrix}\quad [K_0]=\begin{bmatrix}-85.4 & -4.55\\ -4.55 & -1.5\end{bmatrix}$$

$$[K_2]=\begin{bmatrix}0. & 82.6\\ 0. & 4.49\end{bmatrix}$$

Table A1 Bicycle Parameters

	bicycle					
parameter	1	2	3	4	5	6
c	0.068	0.069	0.062	0.072	0.047	0.180
r_R	0.341	0.3410	0.332	0.339	0.341	0.341
r_F	0.343	0.344	0.334	0.330	0.342	0.342
w	1.12	1.12	0.989	1.07	1.09	0.985
IR_{xx}	0.088	0.088	0.055	0.063	0.085	0.085
IR_{yy}	0.153	0.153	0.076	0.101	0.149	0.149
IB_{xx}	11.8	11.4	9.98	9.85	9.03	8.99
IB_{yy}	13.4	12.2	10.3	10.1	9.32	9.27
IB_{zz}	4.30	3.12	2.65	2.65	2.63	2.62
IB_{xz}	-1.67	-1.97	-2.12	-2.07	-2.16	-2.13
IF_{xx}	0.090	0.090	0.055	0.063	0.088	0.088
IF_{yy}	0.149	0.149	0.106	0.106	0.147	0.147
IH_{xx}	0.253	0.253	0.098	0.115	0.145	0.148
IH_{yy}	0.246	0.246	0.069	0.100	0.120	0.119
IH_{zz}	0.096	0.096	0.040	0.023	0.023	0.029
IH_{xz}	-0.072	-0.072	-0.004	-0.018	-0.019	-0.017
m_B	86.7	81.9	76.5	76.5	75.3	75.3
m_F	2.02	2.02	1.58	1.50	1.90	1.90
m_H	3.220	3.22	2.27	2.52	2.45	2.45
m_R	3.11	3.11	1.38	1.94	2.57	2.57
x_B	0.278	0.289	0.296	0.295	0.297	0.296
z_B	-1.03	-1.04	-1.07	-1.073	-1.09	-1.09
x_H	0.867	0.867	0.906	0.960	0.948	0.919
z_H	-0.747	-0.748	-0.732	-0.719	-0.788	-0.816
λ	0.400	0.400	0.276	0.330	0.302	0.339

Table A2 Bicycle Rider Gain Values

		bicycle					
vel	**gain**	1	2	3	4	5	6
2.5	K_δ	22	20.5	22.3	23	18	48
	$K_{\dot{\phi}}$	-0.090	-0.086	-0.130	-0.120	-0.110	-0.070
	K_ϕ	23.3	24.1	15.6	17.7	20.2	27.9
	K_ψ	0.058	0.053	0.662	0.065	0.062	0.063
	K_y	0.195	0.199	0.198	0.198	0.200	0.191
5.0	K_δ	48	43	49	50.5	39	105
	$K_{\dot{\phi}}$	-0.08	-0.087	-0.080	-0.084	-0.085	-0.070
	K_ϕ	9.03	8.50	8.06	8.26	8.61	8.90
	K_ψ	0.161	0.173	0.170	0.168	0.160	0.165
	K_y	0.097	0.100	0.101	0.100	0.101	0.100
7.5	K_δ	74	68	80	82	61	170
	$K_{\dot{\phi}}$	-0.063	-0.060	-0.058	-0.062	-0.063	-0.050
	K_ϕ	6.31	6.74	5.82	5.83	6.34	6.45
	K_ψ	0.332	0.330	0.321	0.315	0.345	0.300
	K_y	0.065	0.065	0.066	0.065	0.065	0.066

Reference

[A1] Meijaard, J., Papadopoulos, J., Ruina, A., and Schwab, A., "Linearized Dynamics Equations for the Balance and Steer of a Bicycle: A Benchmark and Review," *Proceedings of the Royal Society A: Mathematical, Physical and Engineering Sciences*, Vol. 463, No. 2084, pp. 1955-1982, 2007.

Figures

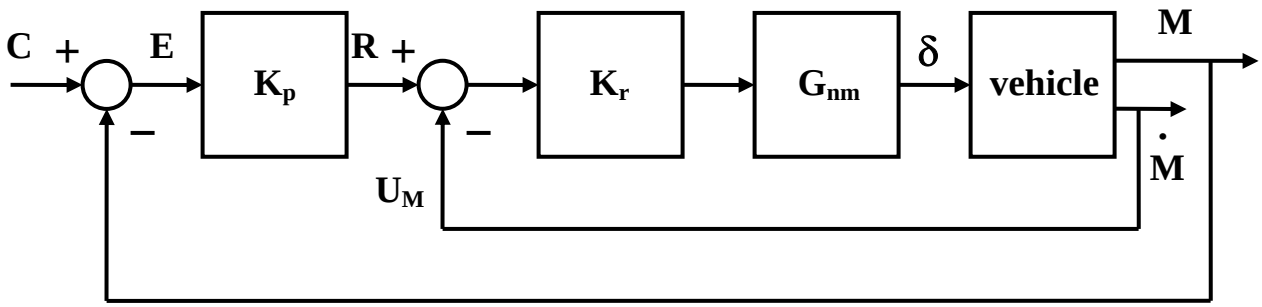

Figure 1 A model of human pilot control behavior.

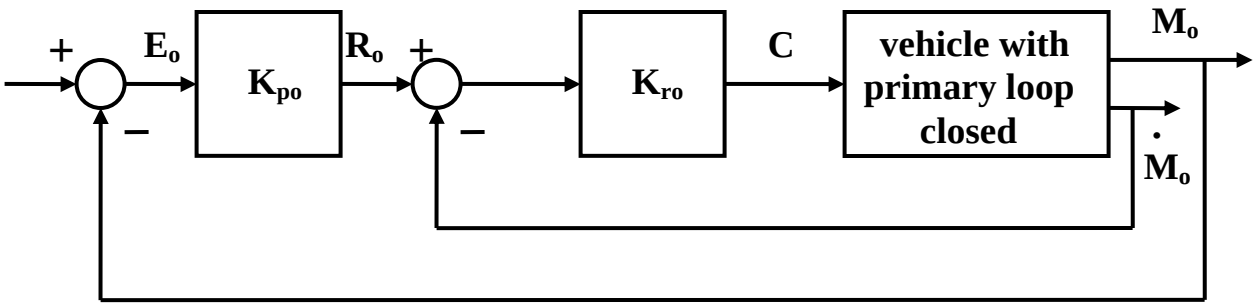

Figure 2 A model of human pilot control behavior in a multi-loop task.

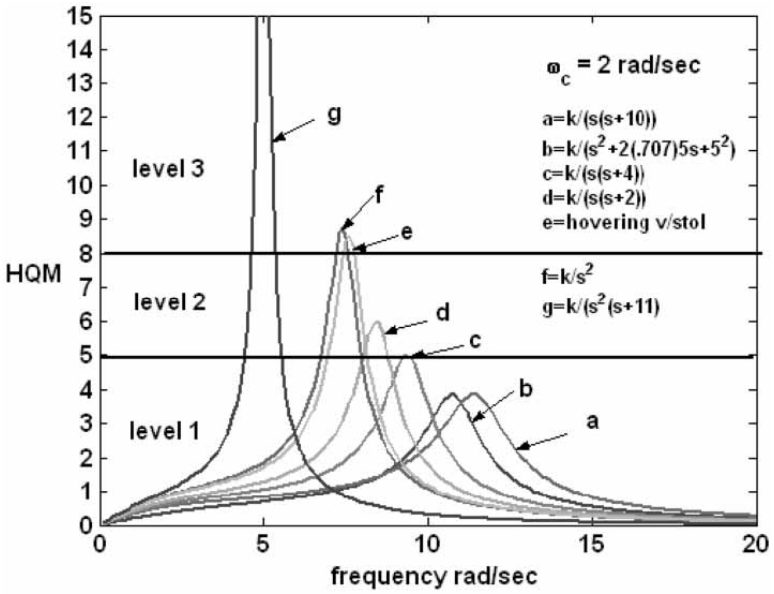

Figure 3 The Handling Qualities Metric from [13].

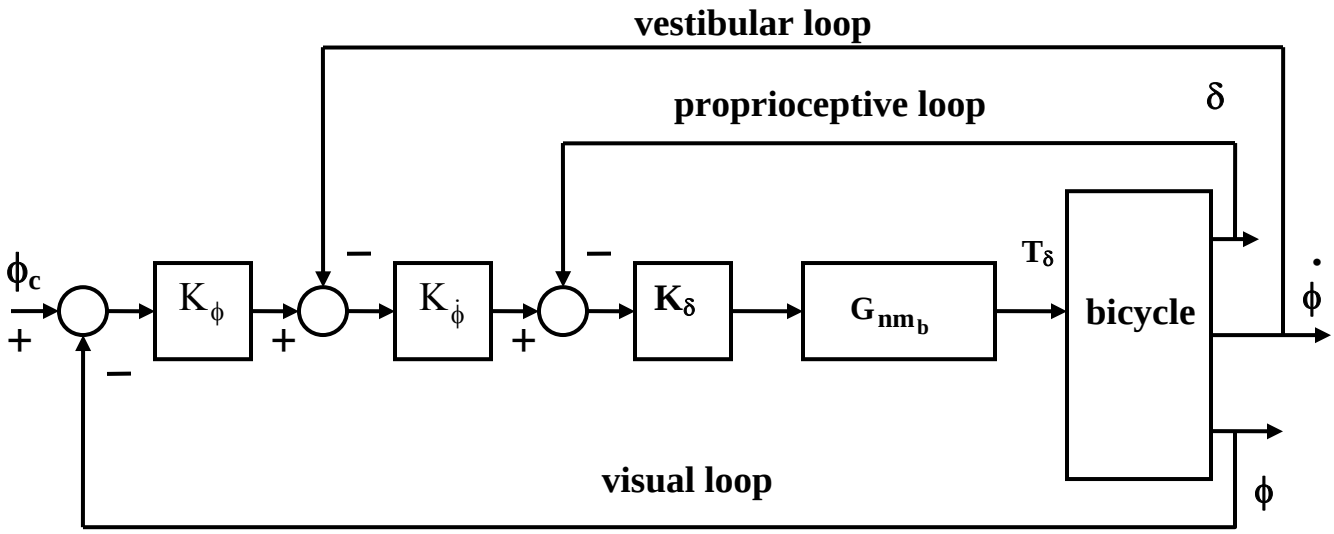

Figure 4 The bicycle rider control model.

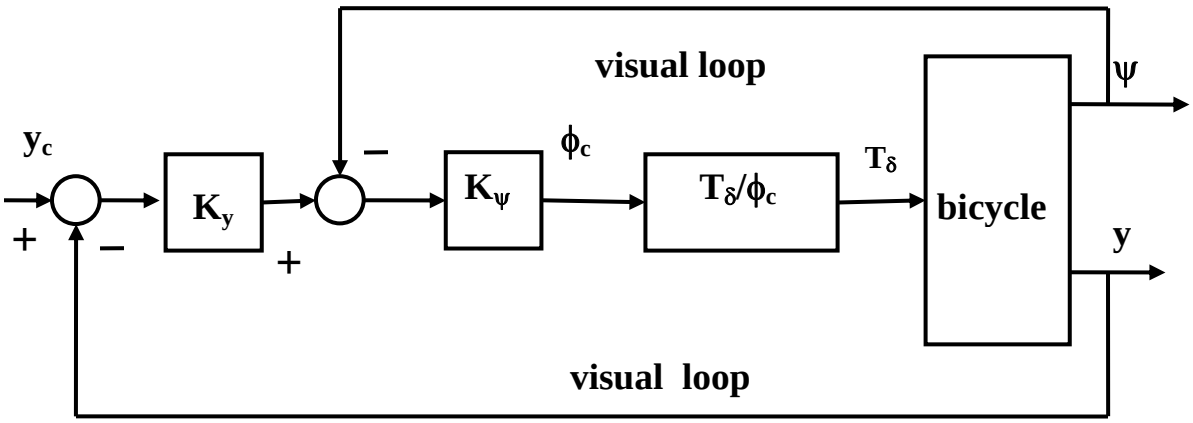

Figure 5 The complete rider/vehicle model.

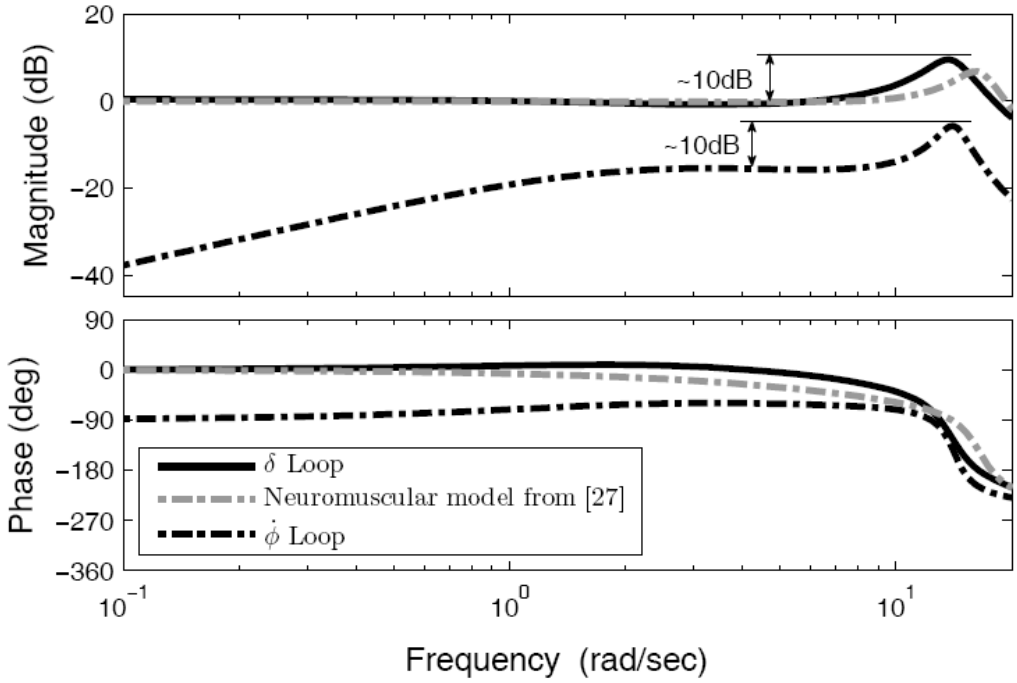

Figure 6 Bode diagrams of the δ and $\dot{\phi}$ closed-loop transfer functions from Fig. 4 and the neuromuscular model from [27].

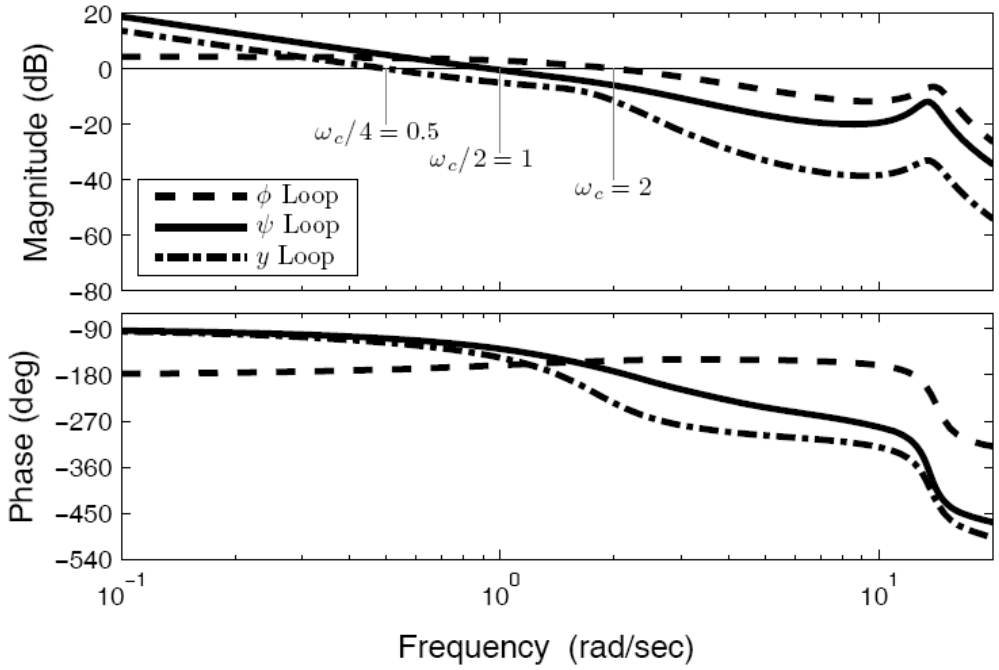

Figure 7 Bode diagrams of the ϕ, ψ, and y open-loop transfer functions from Fig. 6.

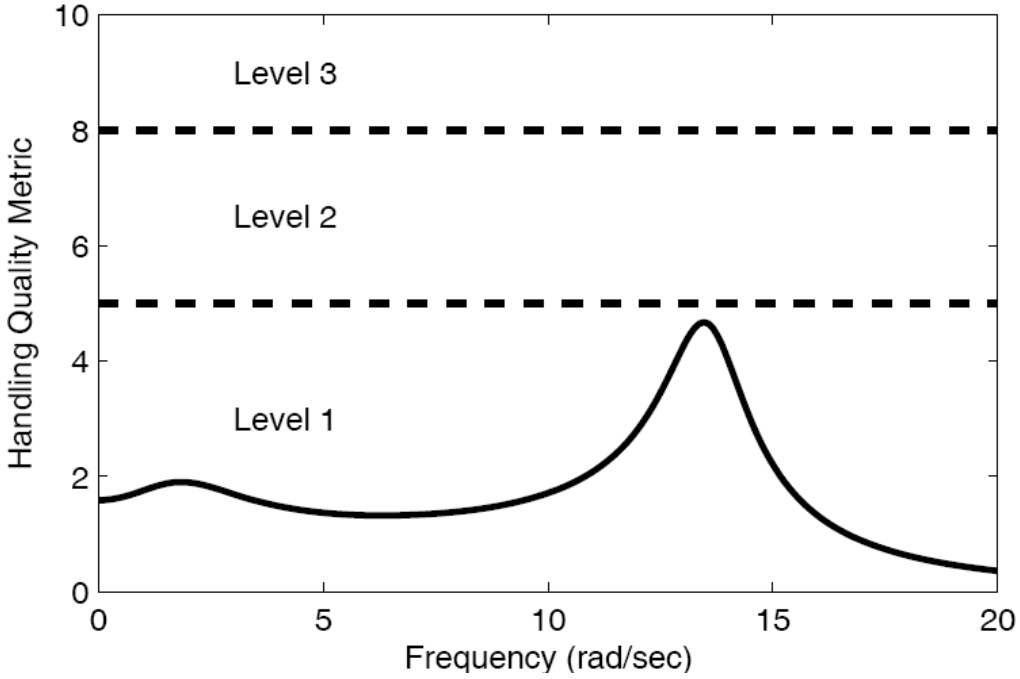

Figure 8 HQM results for the bicycle of Eq. 8.

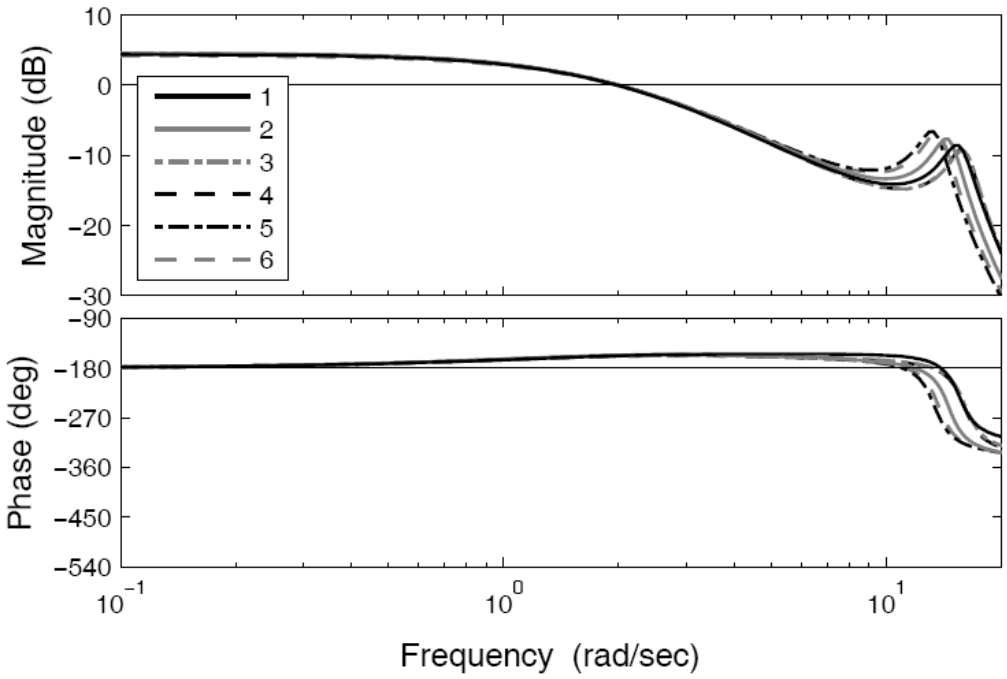

Figure 9 Bode diagram of the ϕ open-loop transfer functions for six bicycles of Appendix, v = 5.0 m/sec.

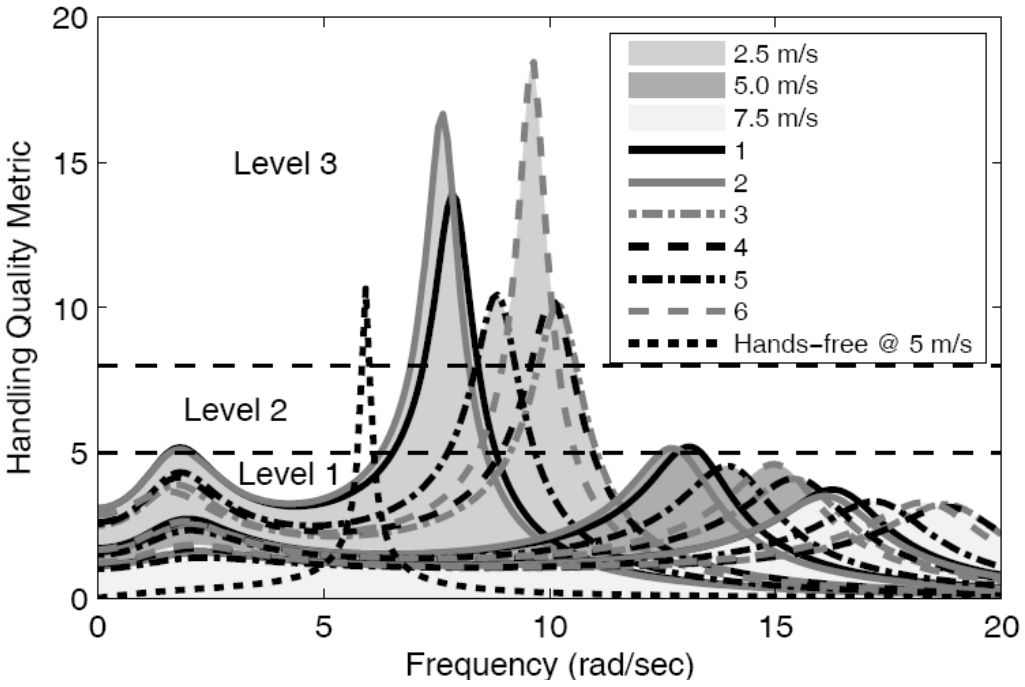

Figure 10 HQM results for six bicycles of Appendix, v = 2.5 m/sec, 5.0 m/sec, and 7.5 m/sec

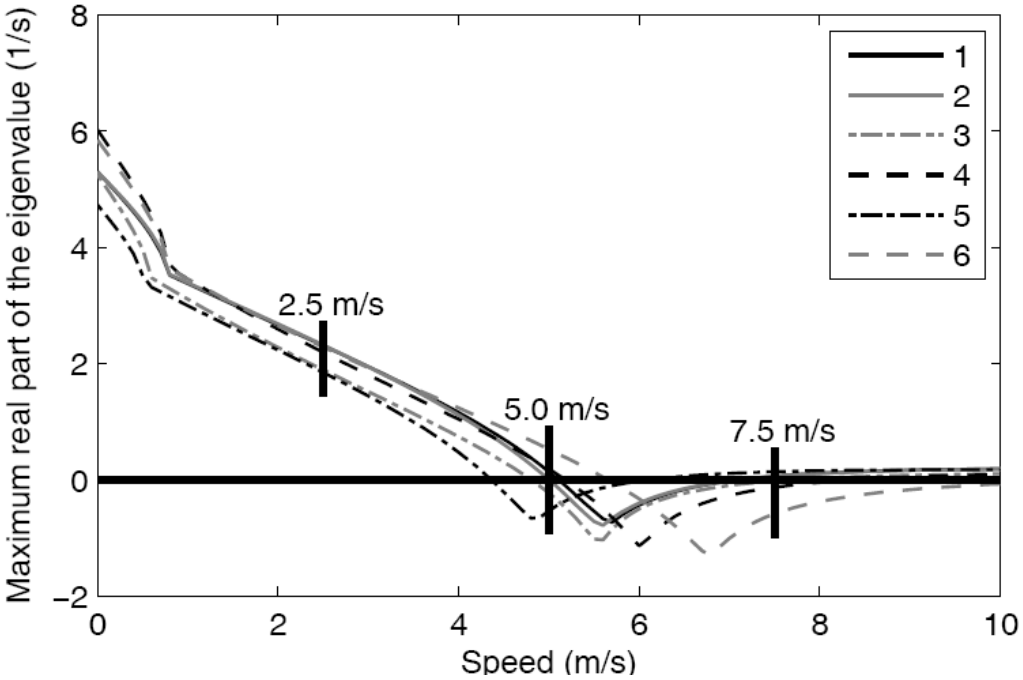

Figure 11 Maximum real part of eigenvalues for each bike across velocities.

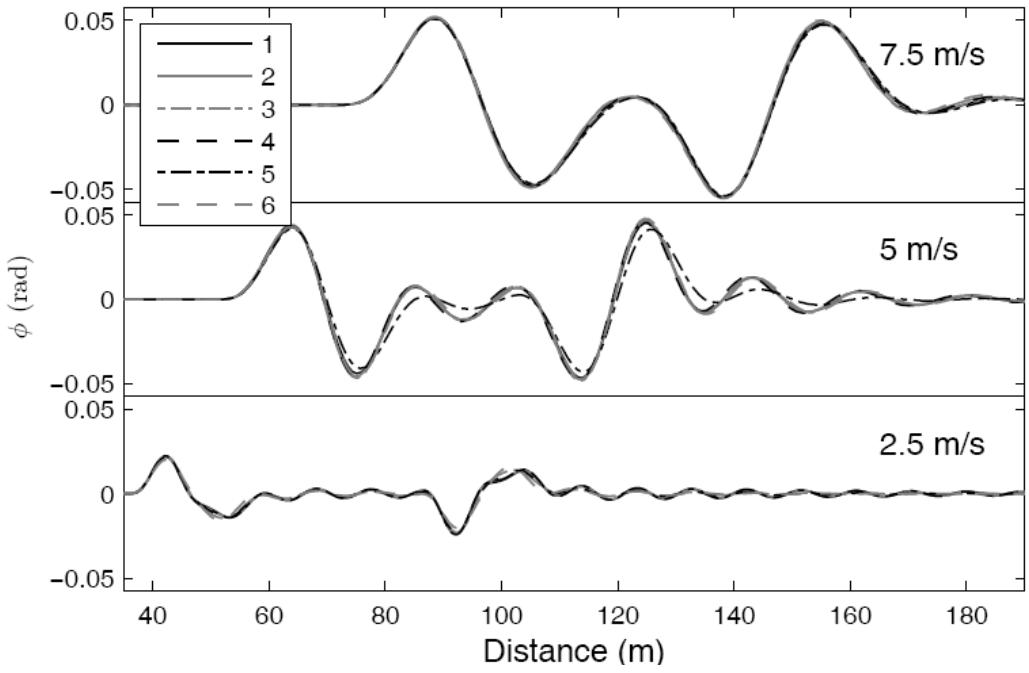

Figure 13 Roll response for six bicycles of the Appendix, v = 2.5 m/sec, 5.0 m/sec, and 7.5 m/sec.

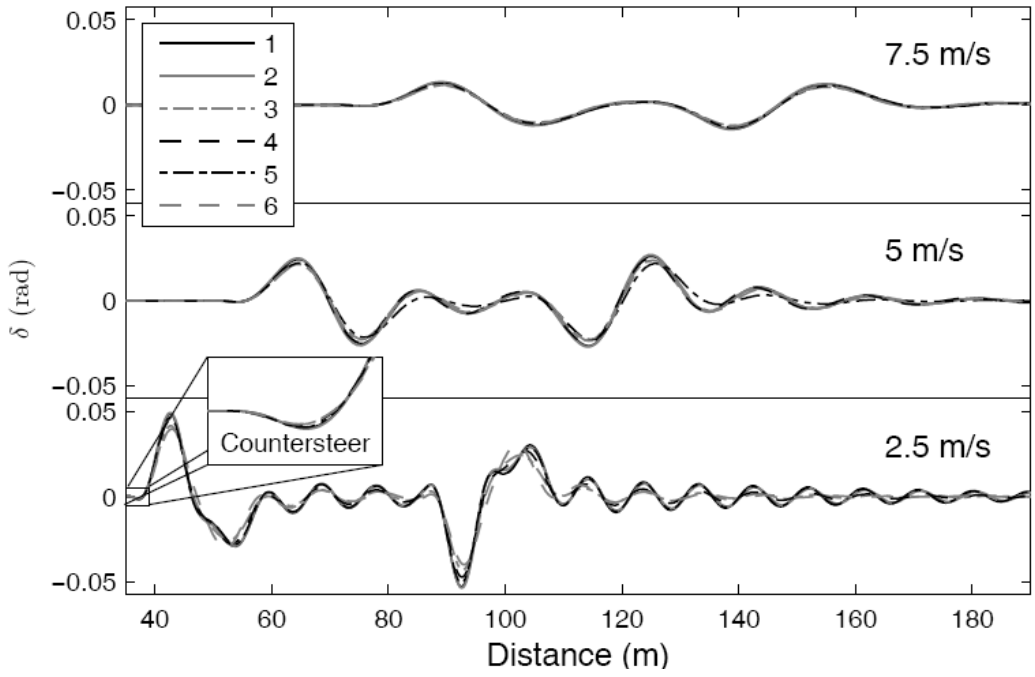

Figure 14 Steering inputs for six bicycles of the Appendix, v = 2.5 m/sec, 5.0 m/sec, and 7.5 m/sec.

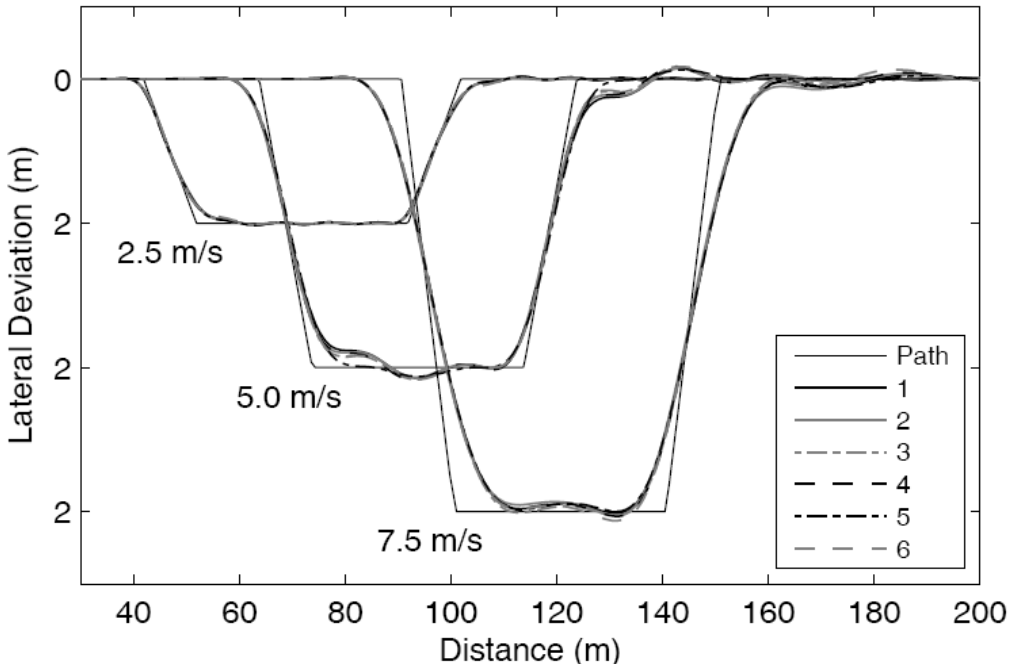

Figure 12 Path tracking performance for six bicycles of the Appendix, v = 2.5 m/sec, 5.0 m/sec and 7.5 m/sec.

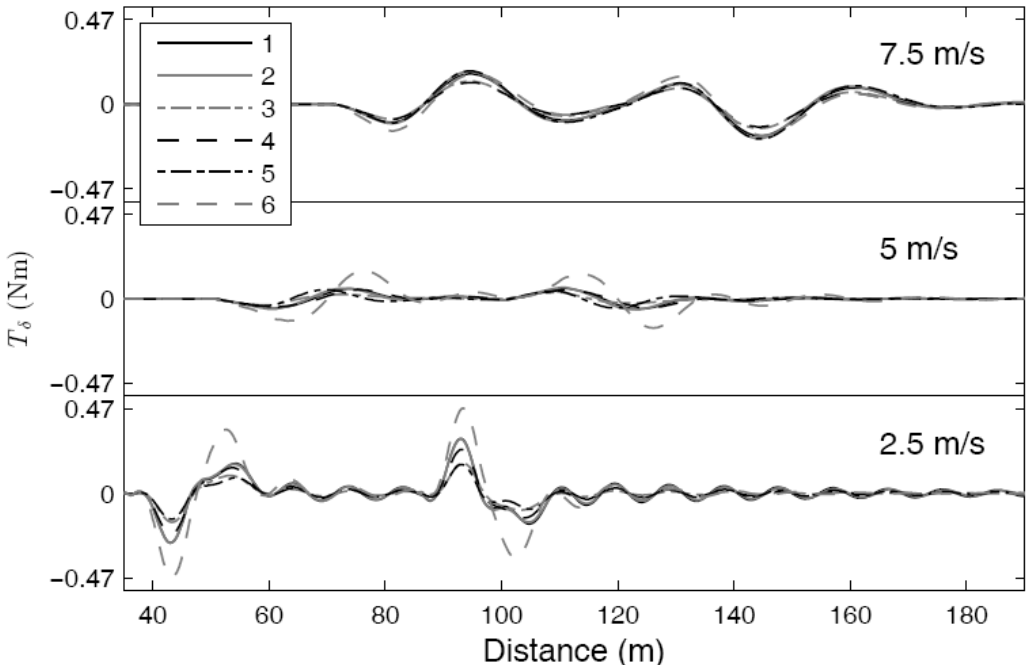

Figure 15 Steering torques for six bicycles of the Appendix, v = 2.5 m/sec, 5.0 m/sec, and 7.5 m/sec.

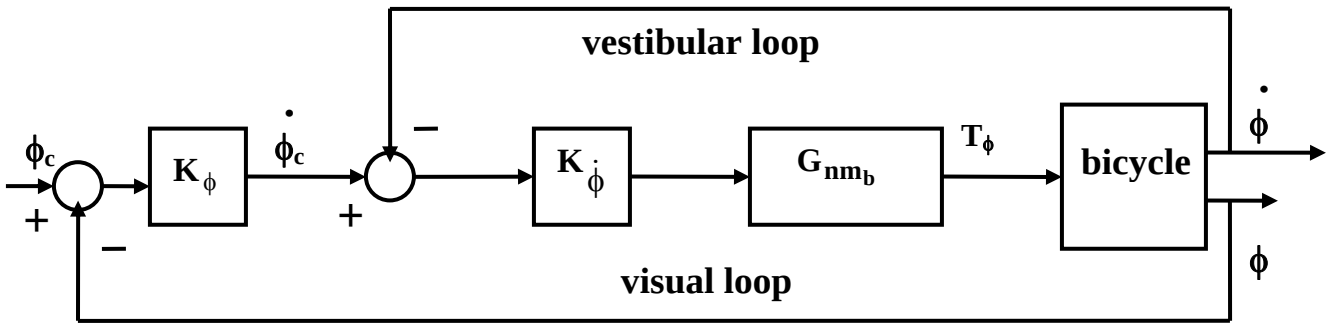

Figure 16 A proposed bicycle rider control model for hands-free riding.

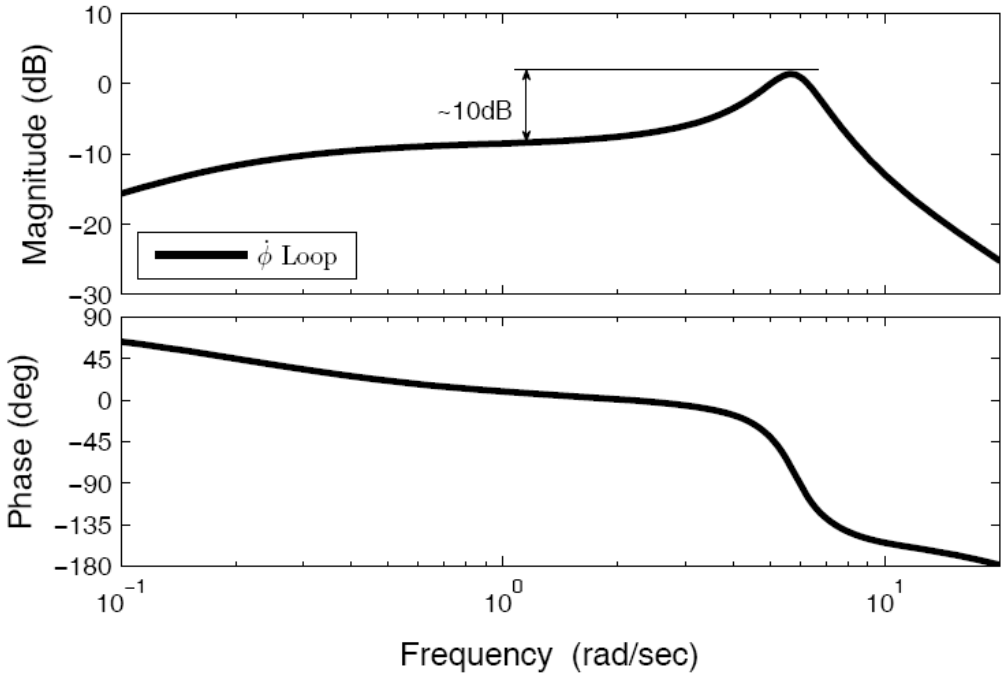

Figure 17 Bode diagram of the inner-most closed-loop transfer function from Fig. 16.

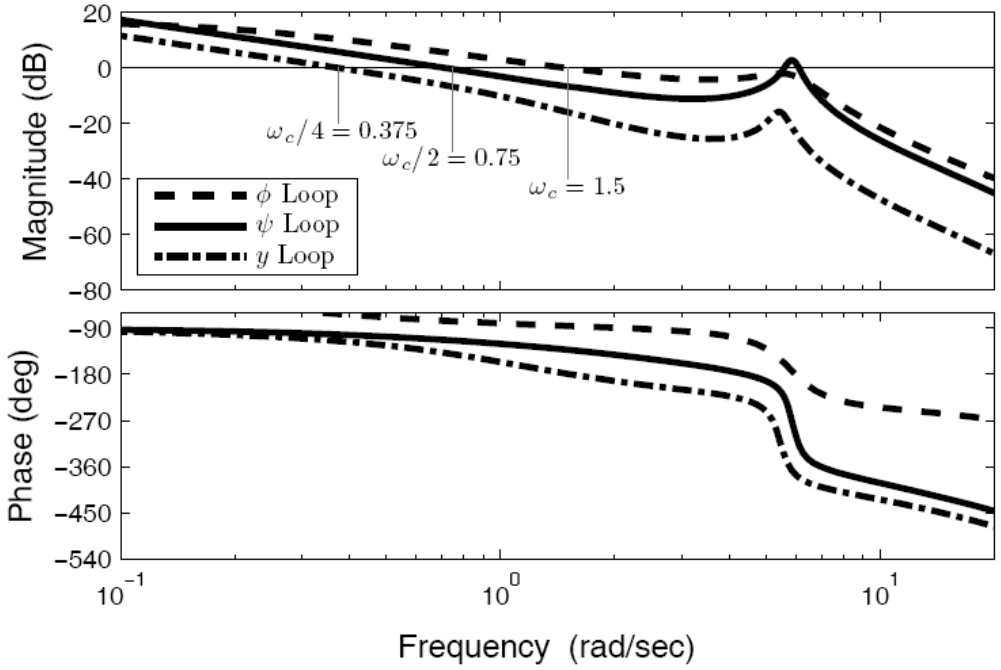

Figure 18 Bode diagrams of the ϕ, ψ, and y open-loop transfer functions for the hands-free rider.

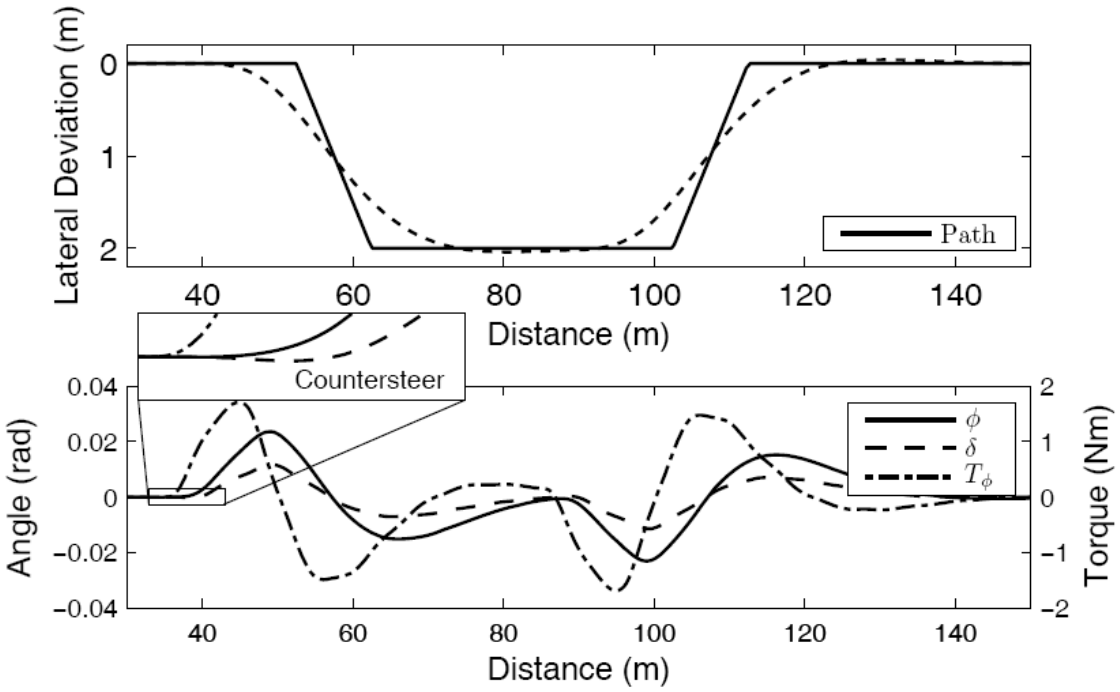

Figure 19 Path tracking, roll response, steering input and "lean" torque for the hand-free case, v = 5.0 m/sec.

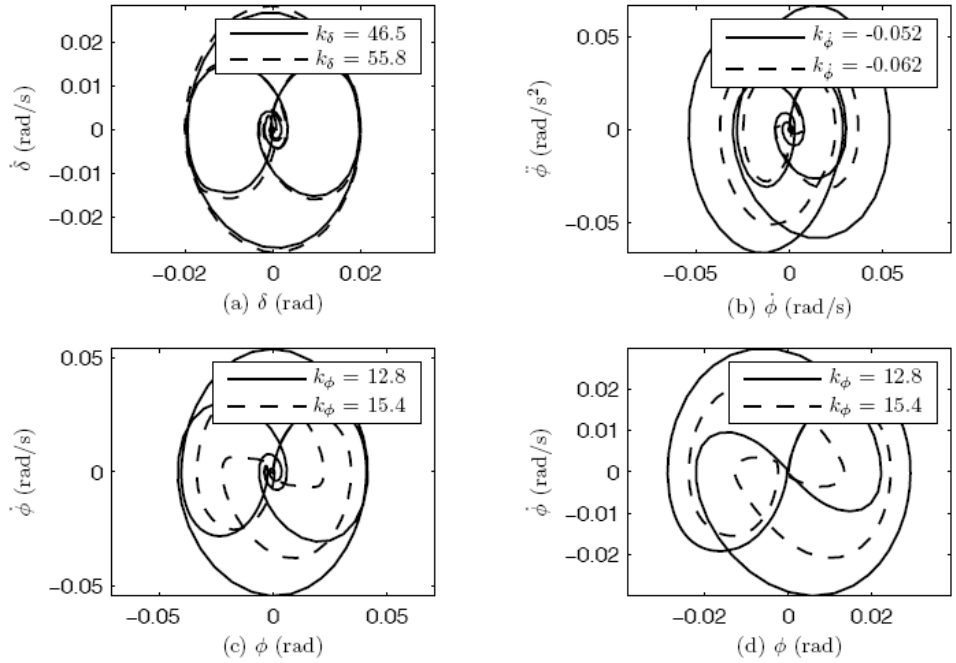

Figure 20 Phase plane portraits for four control loops of Fig. 4.

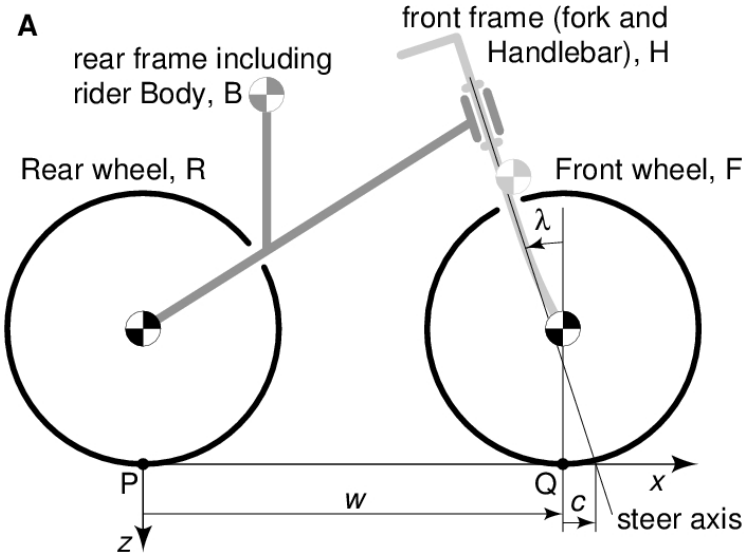

Figure A1 Bicycle geometry (from [A1]).